CHROM. 25 410

Timescales of transient processes in capillary electrophoresis

Eric V. Dose[*] and Georges Guiochon[*]

Department of Chemistry, University of Tennessee, Knoxville, TN 37996-1501 (USA) and Analytical Chemistry Division, Oak Ridge National Laboratory, Oak Ridge, TN 37831-6120 (USA)

ABSTRACT

We apply numerical simulation based on fundamental physical properties to the study of the development of electroosmotic flow and thermal gradient formation that occur immediately after a potential is applied to a capillary filled with electrolyte. Electroosmotic flow requires a few hundred microseconds to develop. We confirm others' findings that radial thermal gradients are generally too small to dominate zone dispersion for capillaries with lumen diameters smaller than about 100 μm. The radial thermal gradient within the capillary lumen requires a few milliseconds to develop, but the general, whole-capillary temperature rise requires ten to a thousand times longer. We combine on one scale the major time-dependent processes that occur when an axial potential gradient is applied, and we demonstrate the theoretical feasibility of using modulated driving potentials to suppress thermal zone broadening.

INTRODUCTION

Much current interest in theory and practice of capillary electrophoresis (CE) is driven quite properly by the technique's very high efficiency. Experiments generally develop over 100 theoretical plates per second, as expected from steady-state theory. However, transient processes in CE resulting from altering the applied potential are not nearly as well understood. When this potential is first applied at the beginning of a CE separation, several changes occur in the capillary including propagation of the electric field down the length of the column, capacitative charging of the double layer at the silica-electrolyte interface, resistive heating of the electrolyte and subsequent development of thermal gradients in the electrolyte and silica, and the start of electroosmotic flow, if any. Also, in real instruments the power supply and electrolyte together constitute a low-pass electric filter so that the potential gradient in the capillary lumen requires some time to rise to the steady-state gradient magnitude.

Each of these processes has a characteristic timescale, and these timescales cover a range of roughly ten orders of magnitude. However, when two or more of these processes have similar timescales, the processes probably interact. The effect of a given process on separation efficiency is probably most complex when its timescale is on the same order as the characteristic time for an analyte molecule to diffuse through the zone either radially (through the distance from the capillary center to the lumen wall or *vice versa*) or axially (from one end of an analyte zone to the other).

We examine below the progress of two major transient processes that occur immediately after a potential is applied to a capillary filled with electrolyte. First, we show that electroosmotic

---

* Corresponding author. Address for correspondence: Department of Chemistry, University of Tennessee, Knoxville, TN 37996-1501, USA.
* Present address: Ross Laboratories, Analytical R&D, 625 Cleveland Avenue, Columbus, OH 43215, USA.

flow does not develop immediately after poten-
tial is applied but that it requires a few hundred
microseconds to develop. Second, we use nu-
merical simulation based directly on very fun-
damental physical assumptions to confirm others'
findings [1–3] that radial thermal gradients are
generally too small to dominate zone dispersion
for capillaries with lumen diameters smaller than
about 100 μm. Finally, we combine on one scale
the relative rates of several transient processes in
CE and comment on the feasibility of using
modulated driving potentials to suppress thermal
zone broadening. In the interests of clarity we
present our methods and results for each process
before proceeding to the next.

NUMERICAL SIMULATION OF ELECTROOSMOTIC FLOW CHANGES

Methods

This simulation is based on the integration of
simple differential equations in one spatial (ra-
dial) dimension. The boundary conditions in the
radial dimension simply consist of the initial
electrolyte velocity (V) at all radii (r) in the
lumen, or $V(t = 0; r)$. Boundary conditions in the
time dimension consist of time history of the
axial flow velocity just inside the aqueous-silica
surface at the wall of the lumen, or $V(t; r = r_{aq})$,
which is the same as the equilibrium flow rate
across the lumen. In fact, we divide the lumen
space into N_{aq} concentric annuli each of thick-
ness Δr, so that the boundary conditions are
specified as $V(t = 0; i)$ and $V(t; N_{aq} + 1)$.

We based the electroosmotic simulations on
some simplifying assumptions. We include no
temperature dependence of the electrolyte vis-
cosity because, as we show below, the timescale
of relaxation of the electrolyte velocity is much
shorter than heating timescales at the lumen wall
so that the viscosity is nearly constant over the
time required to reestablish velocity steady state.
Thus, while electrolyte heating certainly does
alter electroosmotic flow rates [4–7], that process
is slower than the one investigated here. Further,
we assume that the slipping zone at the wall, that
is the very thin boundary layer of electrolyte
solution where the electrolyte velocity increases
from zero at the silica wall itself to the asymp-

totic electroosmotic velocity, is very small com-
pared to the lumen diameter. This assumption is
supported by the very small depth, on the order
of 10 nm, that one calculates for the double layer
in concentrated electrolytes [8–10]. Though
there exist reports that the double layers may
effectively be as thick as 1 or 2 μm [11], even
this would directly affect only the very outermost
annuli in our model, and the timescale indicated
by the model would probably not be affected
significantly.

Integration resolution Δr in the radial dimen-
sion was chosen to be 0.25–1.0% of the lumen
(inside) diameter for electroosmotic simulations.
The propagation of axial velocities was assumed
to arise by simple diffusion through the action of
viscous forces $\vec{F}_i$ per unit length transmitted
through interannulus interfaces i (which lie be-
tween annuli i and $i + 1$) as

$$\vec{F}_i = 2\pi i \eta (V_{i+1} - V_i) \tag{1}$$

which depends on axial velocities V_i and V_{i+1} in
adjacent annuli i and $i + 1$. These forces cause
accelerations $\dot{V}_i$ in annulus i

$$\dot{V}_i = \frac{\vec{F}_i}{M_i} \qquad \text{for } i = 1 ,$$

$$= \frac{(\vec{F}_i - \vec{F}_{i-1})}{M_i} \quad \text{for } 1 < i \leqslant N_{aq} \tag{2}$$

where M_i is the mass of electrolyte in annulus i.
Integrating $\dot{V}_i$ in each annulus from its initial
velocity $V(t = 0; i)$ gives the history of its velocity
V_i.

The integration time increment Δt_{max} depends
on Δr and was computed as one-half the maxi-
mum time during which, given each annulus's
calculated accelerations integrated forward
linearly in time, no annulus's velocity may ex-
trapolate past the mean velocity of its two
adjacent rings. To calculate this, consider a
radial velocity discontinuity between two annuli,
calculate the viscous force in the interface be-
tween them, calculate the initial acceleration of
the electrolyte in one of the two annuli, double
the acceleration to account for the possibility of
an equally large velocity discontinuity on the
other side of the annulus, compute the time for

the electrolyte in this annulus to accelerate by half the initial velocity difference in the discontinuity and halve the time for safety. By this method, the maximum time increment is

$$\Delta t_{max} = \frac{(\Delta r)^2 d}{8\eta} \qquad (3)$$

where d is the electrolyte density and η is the electrolyte viscosity. Note that Δt_{max} is time-independent and need be computed only once before integration begins. Were the integration time increment to exceed Δt_{max}, oscillation and simulation instability would rapidly result. Restricting the time increment to less than Δt_{max} always prevented this oscillatory instability in our work.

Results and discussion

When the electrolyte velocity at the capillary wall suddenly changes because of the application of electrical potential down .the capillary axis, viscous forces accelerate the bulk of the electrolyte until the electrolyte all moves in plug flow at the same velocity as the electrolyte at the wall, as expected. This radial propagation occurs at a rate proportional to the electrolyte solution's kinematic viscosity, or its intrinsic viscosity divided by its density. By taking advantage of the analogy between wall-driven electroosmotic flow propagation and well-thermostatted heat transfer, we calculate a characteristic relaxation time for this process as

$$t_{char} = \frac{R_{aq}^2}{\alpha_1^2 (\eta/d)} \qquad (4)$$

where α_1 is the first root of the Bessel equation $J_0(\alpha) = 0$, about 2.4048 [12]. For a capillary of inside diameter 50 micrometers filled with an electrolyte similar to water at room temperature is about 110 μs. From our simulation results given in Fig. 1 it is clear that the electroosmotic flow has in fact regained its radial uniformity by 200 to 300 ms after potential is initially applied. Eqn. 4 also predicts that the electroosmotic relaxation time is proportional to the square of the capillary inside diameter, and simulation results like those in Fig. 2 are consistent with this expectation.
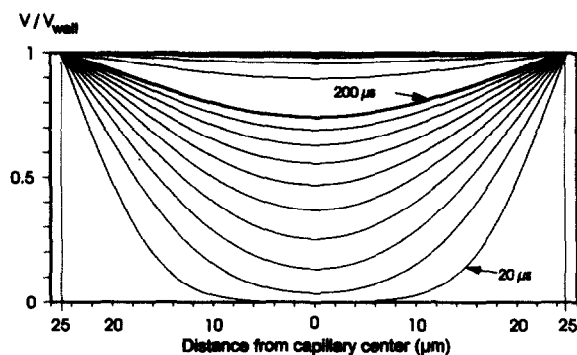

Fig. 1. Axial electrolyte velocity profiles at 20, 40, 60, . . ., 180, 200 (bold curve), 300, 400, and 500 μs after potential applied.

Except for instruments designed specifically to induce high-frequency, high-voltage potential changes in the capillary, most CE instruments will have rise times considerably longer than 1 ms [13]. The present analysis concludes that for these usual instruments, electroosmotic flow effectively propagates instantaneously across the capillary lumen, and electroosmotic flow delays generally need not be taken into consideration. This process appears to be faster than all thermal and all other transient mechanical processes in CE. This is especially true for capillaries with very small inside diameters [14,15].

Even for an instrument with zero potential gradient rise time, the zone broadening effects of electroosmotic relaxation are small. Because analyte molecular diffusion is much slower than effective velocity–propagation diffusion (whose effective diffusion coefficient is equal to the
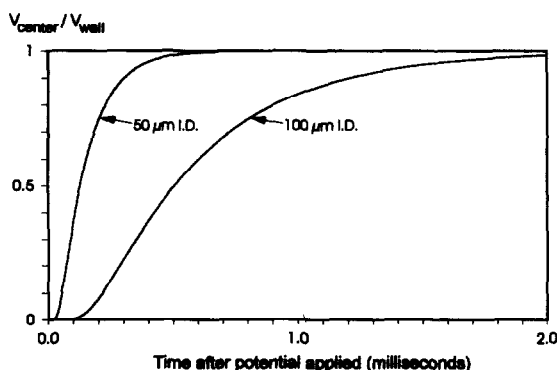

Fig. 2. Axial electrolyte velocity profiles at the lumen center.

kinematic viscosity, about 10^{-2} cm^2/s for water), electroosmotic relaxation will have its full effect on the analyte's radial concentration profile before diffusion can significantly blur it.

The zone broadening effect of electroosmotic relaxation during a cycle where the potential is applied and withdrawn could therefore be measured in principle by moving an analyte zone past the detector and measuring the zone's breadth (variance), applying one or more axial potential changes each separated from the next by enough time to allow radial diffusional mixing, and then moving the zone back across the detector to measure the peak variance increase. Performing this experiment by numerical simulation on a column of inside diameter 50 μm, one measures the axial zone variance introduced for one voltage-switching cycle as about 0.4 V_{EO} micrometers^2, where V_{EO} is the electrolyte velocity at the wall in cm/s. We also find that this axial variance induced by electroosmotic relaxation is proportional to the fourth power of the capillary inside diameter. Voltage-switching variance contributions calculated in this way are five orders of magnitude smaller than upper limits previously deduced by experiment [16], suggesting either that some addition source of voltage-switching dispersion exists or that determination of dispersion by subtraction of calculated variance contributions from measured zone variances is inherently difficult. It is also possible that heterogeneity of the silica surface and therefore of its zeta potential is more important than is the observed (average) rate of electroosmotic flow itself. Though it is clear that neither ideal electroosmotic flow nor its modulation causes much zone broadening, electroosmotic flow heterogeneity may be inevitable whenever electroosmotic flow exists at all, and this may be the reason electroosmotic flow is often observed to lower the plate count to a fraction of that expected.

NUMERICAL SIMULATION AND THERMAL CHANGES

Methods

For cases where the temperature coefficient of electrolyte conductivity is nonzero, the radial temperature profile in a capillary heated by power dissipation in the lumen is solvable to any desired degree of accuracy only by numerical simulation [17]. As in the electroosmotic problem in the previous section, we divide the space within the capillary's outer wall into concentric annuli each of thickness Δr, the radial integration resolution, chosen to be 0.25–1.0% of the capillary outside diameter. The model could be adapted to rectangular capillaries [18–20] or etched channels [21–22] with some loss of simplicity. For thermal simulations the boundary conditions in the space dimension consist of initial temperature (T) at all annuli i in the capillary, or $T(t = 0; i)$, and the boundary conditions in the time dimension consist of the history of the temperature of the air at the polyimide-air interface, or $T(t; r = N_{pi} + 1)$, where N_{pi} is the total number of annuli representing the space within the capillary lumen, silica, and polyimide coating.

We made some simplifying assumptions in the thermal simulations. First, we set to zero the temperature coefficients of thermal conductivities Λ_{th}, specific heats C_p, and densities D for electrolyte, silica, and polyimide coating and we assumed that there is little double layer reorganization after application of the axial potential, though there may be experimental evidence in favor of some very slow such processes [23]. We assumed that the thermal transfer coefficient to air was temperature-independent, though the temperature of the outer capillary wall is very difficult to measure, as noted in other work [6]. We assumed that the temperature of the capillary's surroundings are radially symmetric [24] and held constant at a known temperature; real instruments will satisfy this assumption to varying extents [25]. We ignore radiative heat losses [26] and surface conductivity at the double layer [10], each of which is expected to be very small. Finally, electrolyte conductivity temperature dependence in a given simulation was assumed to be either linear

$$\Lambda_{th}(T) = \Lambda_{th}(T_0)(1 + j(T - T_0)) \tag{5}$$

or exponential

$$\Lambda_{th}(T) = \Lambda_{th}(T_0)e^{j(T-T_0)} \tag{6}$$

in form, where T_0 is the temperature of the capillary's surroundings, and j is the temperature coefficient of electrical conductivity at T_0

$$j = \frac{1}{\Lambda_{th}(T_0)} \cdot \frac{d\Lambda_{th}}{dT} (T_0) \qquad (7)$$

The value of j is usually about 0.02 [27]. We used exponential temperature dependence except in simulations intended to model previously published work which employed linear or zero temperature dependence. When comparing our results to those of other work we adopted all capillary dimensions and physical properties used in that work.

The enthalpy rate of change $\dot{H}_{IR,i}$ generated by electrical resistance per unit length within each annulus i is

$$\dot{H}_{IR,i} = \begin{cases} (2i+1)\pi(\Delta r)^2 E^2 \Lambda_{IR} & \text{for } i \leq N_{aq}, \text{ and} \\ 0 & \text{for } i > N_{aq} \end{cases} \qquad (8)$$

where E is the axial potential gradient (electrical field), Λ_{IR} is the electrolyte's electrical conductivity, and N_{aq} is the number of annuli representing the lumen space. The outward heat flux F_i per unit length across each boundary i (which lies on the outside surface of annulus i) is

$$F_i = \begin{cases} 2\pi i[T_i - T_{i+1}]\bar{\Lambda}_{th} & \text{for } i < N_{pi}, \text{ and} \\ 2\pi R_{pi}h & \text{for } i = N_{pi} \end{cases} \qquad (9)$$

where T_i and T_{i+1} are the temperatures in annuli i and $i+1$, $\bar{\Lambda}_{th}$ is the mean thermal conductivity of the materials in annuli i and $i+1$, h is the extrinsic heat transfer coefficient from the outside to the capillary's polyimide coating to the surrounding medium, and R_{pi} is the capillary outside radius. Thus the total enthalpy rate of change $\dot{H}_i$ per unit length for annulus i is

$$\dot{H}_i = \begin{cases} -\Delta F_{H,i} + \dot{H}_{IR,i} & \text{for } i = 1, \\ \Delta F_{H,i-1} - \Delta F_{H,i} + \dot{H}_{IR,i} & \text{for } 2 \leq i \leq N_{pi} \end{cases} \qquad (10)$$

and the rate of temperature change $\dot{T}_i$ in annulus i is

$$\dot{T}_i = \frac{\dot{H}_i}{\pi(2i-1)(\Delta r)^2 D_i C_{p,i}} \qquad (11)$$

Given an integration cycle time increment Δt (see below), the temperature change ΔT_i resulting from one integration cycle for each annulus i is

$$\Delta T_i = \dot{T}_i \Delta t \qquad (12)$$

For thermal simulations, the integration time increment Δt_{max} must be no greater than the lesser of two upper limits. The first prevents integration oscillation in the same manner as does eqn. 3 described above and is given by

$$\Delta t_{max}(1) = (\Delta r)^2 \min\left(\frac{d_i C_{p,i}}{4\Lambda_{th,i}}\right) \quad \text{over } 1 \leq i \leq N_{pi} \qquad (13)$$

where $C_{p,i}$ is the heat capacity and $\Lambda_{th,i}$ is the thermal conductivity within a given annulus i. Under the simplifying assumptions above, $\Delta t_{max}(1)$ is time-independent and need be computed only once before integration begins. The second limit prevents resistive heating from causing the lumen temperature to increase in one integration cycle by more than an arbitrarily chosen limit ΔT_{max}, so that

$$\Delta t_{max}(2) = \min\left|\frac{\Delta T_{max}}{\dot{T}_i}\right| \quad \text{over } 1 \leq i \leq N_{pi} \qquad (14)$$

We chose ΔT_{max} to be less than about 0.1% of the total temperature rise at the capillary lumen center. Unfortunately, $\Delta t_{max}(2)$ depends on the temperature profile and so must be computed in every integration cycle. Except at extremely high applied power or extremely low arbitrary limit ΔT_{max}, $\Delta t_{max}(1)$ was always smaller than $\Delta t_{max}(2)$ and thus defined the time increment we actually used, but to ensure computational stability we always computed both.

Results and discussion

We first ran our numerical simulations to long times to compare our steady state to results given in various other literature reports. Temperature profiles within the capillary lumen are very nearly parabolic, as noted by other workers

TABLE I

COMPARISON OF PRESENT NUMERICAL SIMULA-
TION (A) WITH ANALYTICAL APPROXIMATION OF
REF. 25 (B)

Zone	Percent of total temperature range falling within given zone (%)	
	A	B
Electrolyte	2.7	2.7
Silica wall	2.8	2.8
Polyimide coating	1.3	1.4
Air–polyimide interface	93.2	93.1

TABLE II

COMPARISON OF PRESENT NUMERICAL SIMULA-
TION (A) WITH ANALYTICAL APPROXIMATION OF
REF. 27 (B)

Lumen radius (μm)	Lumen temperature range (K)		Lumen wall temperature (K)	
	A	B	A	B
25	0.33	0.53 (0.35?)	299.1	299.0
50	1.37	1.39	301.5	301.2
75	3.10	3.14	304.8	304.2
100	5.52	5.58	308.8	307.7
125	8.64	8.72	313.2	311.6

[28], though exceptions may exist [29]. Using the physical parameters of Table II of ref. 26, we obtain steady state profiles (Table I) that agree closely with those obtained from the analytical approximation given in ref. 26. In Table II we show that our numerical results agree with other analytical approximations over a wide range of capillary lumen radii (we suspect that the lumen temperature range of 0.53 K given by ref. 28 for lumen radius 25 μm is a typographical error because it is inconsistent with other results in the same table). The steady-state temperature profile we obtain from numerical simulation also agrees closely with the results in ref. 30 using the analytical approximations of ref. 30 as given in the last column of our Table III.

Numerical simulation under conditions given in ref. 25 predicts a lumen temperature increase of 5.0°C given thermal transfer coefficients typical of liquid cooling and 1.7°C given perfect thermal dissipation at the outer surface, compared with the *experimental* temperature measurement [25] of 1.9°C, suggesting that if the measurements were accurate, thermal dissipation in those experiments was extremely efficient.

However, it is in the study of non-steady-state thermal behavior that numerical simulation has the greatest advantages. One major advantage is that it provides direct access to simulated thermal profiles at any time during the equilibration process, as illustrated by Fig. 3. Another feature of the numerical approach is its ability to employ any boundary conditions or physical conditions
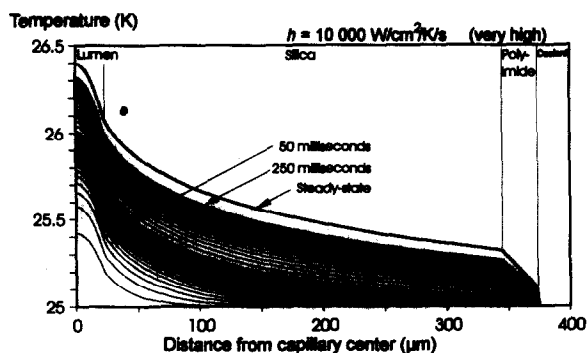
TABLE III

COMPARISON OF PRESENT NUMERICAL SIMULATION (A) WITH ANALYTICAL APPROXIMATION OF REF. 29
(B)

Position (μm from center)	Temperature increase (K)							
	0.034 s		0.34 s		1.36 s		"Steady state"	
	A	B	A	B	A	B	A	B
Center (0 μm)	4.31	4.23	19.1	18.9	28.7	28.4	29.2	28.9
Aqueous–Si (75 μm)	2.52	2.49	16.3	16.0	25.2	24.8	25.2	25.3
Si–polyimide (166 μm)	1.66	1.70	14.7	14.3	22.9	22.6	23.4	22.9
Polyimide–air (180 μm)	1.40	1.49	13.2	13.0	20.6	20.5	20.9	20.9

Fig. 3. Electrolyte velocity temperature profiles at 2, 4, 6, ..., 48, 50, 60, 70, 80, ..., 240 and 250 ms after potential first applied. Simulated conditions as given in ref. 28: capillary radii: lumen 25 μm, silica 345 μm, polyimide 375 μm; potential gradient 300 V/cm; resulting current 88.4 μA.

whatsoever. Especially, one may set any initial temperature conditions one likes, and in fact may integrate backwards in time, though this technique is prone to oscillation because the profile-broadening effects of thermal conduction are reversed. One may include the effects of varying the surroundings' temperature, for example when the thermostatting system has a lag time or is influenced by air conditioning. One may even include sudden, gradual, or cyclical changes in the applied potential, thermal or electrical conductivities, or other physical parameters, though many combinations may not be physical consistent.

The conditions of the separation considered in ref. 28 include extremely efficient thermal transfer from the capillary's outer surface to its surroundings, and as expected most of the steady-state temperature drop is predicted to occur within the silica and the lumen with very little drop at the capillary outer surface (Fig. 3). Temperatures at the interfaces agree with those predicted by analytical means [28]. However, even in this nearly ideal case, the whole-capillary temperature rise takes about 100 times as long to develop as does the parabolic profile in the lumen, even with efficient thermal transfer at the outer surface. The lumen profile is fully developed within a very few milliseconds. Such results confirm the need to distinguish between rates of thermal gradient development within the capillary's inside and outside diameters [26].

Assuming a smaller, more realistic thermal transfer rate h at the outer wall, we find that temperature profiles given by the present numerical simulation method agree at several radial positions and at several time points after first application of axial potential (Table III) with results of analytical approximations previously published [30,31]. Again we find that the parabolic temperature profile shape and gradient magnitude in the lumen develop in the first few milliseconds (Fig. 4). However, in most other ways the development of thermal profiles depends greatly on thermal transfer efficiency at the capillary outer wall —at lower thermal transfer efficiency the temperature rise across the column is much larger in proportion to the power dissipation, a much greater fraction of the temperature gradient across the capillary occurs at the outer surface, and the temperature rise throughout the capillary, including inside the lumen, take longer to complete.

Once thermal steady state is achieved, setting the applied potential to zero reverses the processes (Fig. 5). First, the parabolic temperature profile across the lumen flattens in a very few milliseconds, and the whole capillary cools more slowly and in a nearly exponential fashion.

In the case of very inefficient thermal transfer from the outer surface of a capillary in contact only with still air, almost all of the radial tem-
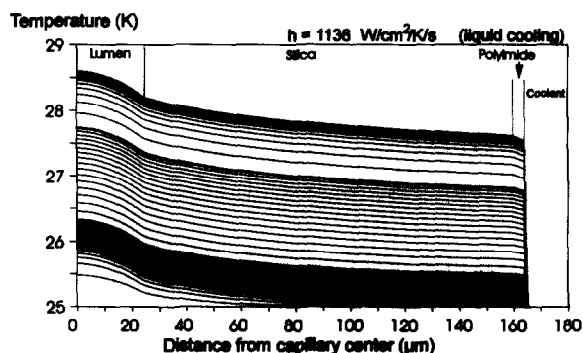

Fig. 4. Electrolyte temperature profiles (beginning with lowermost curve) at 2, 4, 6, ..., 38, 40 (bold curve), 50, 60, ..., 180, 200 (bold curve), 250, 300, ..., and 1000 ms after potential applied beginning at power-off steady state. Simulated conditions after ref. 30: capillary radii: 25 μm, silica 160 μm, and polyimide 165 μm; potential gradient 300 V/cm; resulting current 100 μA.
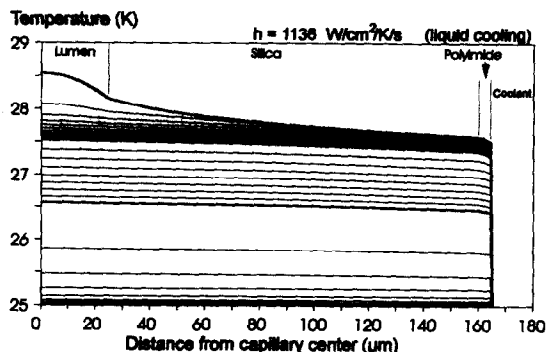
Fig. 5. Electrolyte temperature profiles (beginning with uppermost curve) at 0, 2, 4, 6, . . . , 18, 20 (bold curve), 30, 40, . . . , 90, 100 (bold curve), 200, 300, . . . , and 700 μs after potential set to zero after thermal steady state established. Conditions as in Fig. 4 except that potential gradient and current refer to preexisting steady state.

perature drop occurs at the outer surface (Fig. 6), that is, the temperature profile across the entire capillary is relatively very flat [9,26,27]. The inefficient heat dissipation requires that the applied potential be kept very small so that the temperatures in the lumen are kept low enough to prevent "thermal runaway" caused by positive feedback between temperature rise and electrolyte conductivity increases [24,26] large thermally induced pH changes [32], chemical changes like protein denaturation [27,33] or reduction [33], and other problems. The low power dissipation causes very little parabolic,
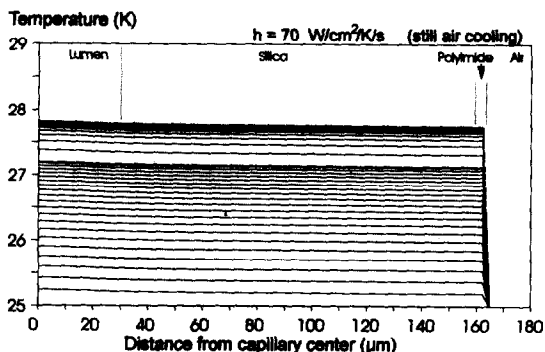

Fig. 6. Electrolyte temperature profiles (beginning with lowermost curve) at 200, 400, 600, . . . , 3800, 4000 (bold curve), 5000, 6000, . . . , and 20 000 ms after potential applied. Simulated conditions after ref. 30: capillary radii: 25 μm, silica 160 μm, and polyimide 165 μm; potential gradient 75 V/cm; resulting current 25 μA.

zone-broadening radial thermal gradient in the lumen, but it also means that ion velocities will be so slow that the electrophoretic analysis will be slow. The capillary's approach to thermal steady state requires several seconds in this case. The use of capillaries with extremely small inside diameters [14,15] helps in two ways: by suppressing thermal broadening by decreasing the parabolic [34], zone-broadening thermal gradients inside the lumen, and simply by decreasing the amount of power that the outer capillary surface is required to dissipate. However, note that at constant electrolyte composition, smaller inside diameters can cause the electric field rise time *in the capillary* to lengthen dramatically [13].) Further, there is experimental evidence [35] that the extent of convection and therefore the effective thermal transfer rate in still air depend on the outer surface temperature in unpredictable ways [36]. Fortunately, in electrokinetic sample injection the injection end of the capillary is immersed in the sample solution, so that the degree of temperature changes and the unpredictability of thermal transfer rates at the injection end of the capillary will not be as important as they might at first appear, though electroosmotic flow changes caused by slow capillary heating during injection may impair quantitative precision.

Thus we confirm by independent means that efficient thermal transfer at the capillary outer walls are required for analyses that require both high separation efficiency and short analysis times. Air-cooled silica capillaries are known to limit the power dissipation to about 1 W/m [37,38] for efficient separations. Our results are consistent with others' findings that efficient capillary cooling over the length of the capillary including near the detector [24] suppresses thermal zone broadening [9] and that under very efficient capillary cooling the thermal zone broadening is smaller than other sources of broadening [2,9,28,30,39] and especially that it contributes less broadening than does the length of the injection zone itself [1–3] in the efficient cooling case. Such efficient thermal transfer also speeds thermal equilibration of the whole capillary (though not of radial thermal gradients in the lumen) so that it is probably especially

important for efficient, quantitative CE separations in short capillaries with large inside diameters and relatively high electrolyte conductivities.

TIMESCALES OF TRANSIENT EVENTS IN CAPILLARY ELECTROPHORESIS

We can now compare the timescales of several transient processes in CE (see Fig. 7). The fastest process is certainly the propagation of axial potential gradients down the length of the capillary lumen. For a capillary of length l filled with electrolyte of refractive index n, this characteristic propagation time is $t_{char} = ln/c$, where c is the speed of light in a vacuum. For a 1 m column filled with aqueous electrolyte t_{char} is on the order of a few nanoseconds, depending on the refractive index of the electrolyte at the effective frequency at which the axial potential is applied. Thus even with the fastest power supplies one need not be concerned with electric field phase changes in a CE capillary. Though ion migration under an abrupt potential gradient change may indeed occur on a picosecond timescale [40], one can do very little to decrease the potential propagation time, so the former timescale must defer to the latter.

Electroosmotic flow radial propagation occurs on the order of hundreds of microseconds as demonstrated above. This relaxation time can be accelerated greatly by increasing the electrolyte solution viscosity, but the most apparent effect will be the suppression of electroosmotic flow altogether.

Thermal changes following application of potential to a CE capillary fall into two categories: the first, which occurs inside the capillary lumen and causes some zone dispersion, and the second one a more general temperature rise over most of the capillary. The relaxation time of the thermal gradient in the capillary lumen is much faster than that of the general temperature rise largely because the distance over which heat must be conducted is much shorter in the first case than in the second; the resistance to heat flow presented by the capillary outer surface also serves to slow the general temperature rise, but not the parabolic profile formation in the lumen.

The relaxation time of the thermal gradient in the lumen depends mostly on the capillary's inside diameter and not on applied potential [2], while the relaxation time of the general temperature rise depends greatly on the efficiency of heat transfer at the outer surface of the capillary, and to a lesser extent on the capillary outside diameter. Inefficient heat removal from the capillary's outer surface may cause serious quantitation problems in electrokinetic injection by making non-linear the relation of analyte amount injected with the product of injection voltage and duration of injection. Convective cooling in unstirred air worsens this problem still more because the surface thermal transfer coefficient h probably depends in complex ways on the capillary surface temperature [36].

The electric field rise time in the capillary lumen is probably the most readily controlled of the transient processes considered in this work [3,40]. Though it is probably in the hundreds of milliseconds in most instruments, with care this rise time can be shortened to the millisecond range [13]. This electric field rise time in the capillary makes irrelevant all clearly shorter rise times.

Analyte diffusion across the lumen is the only process whose timescale depends directly on analyte properties, specifically on the analyte diffusion coefficient D_x. This process's timescale is the most variable of those considered in this work. The diffusion coefficient is directly calculable from the measured signed mobility m_x and charge Z_x of analyte x as
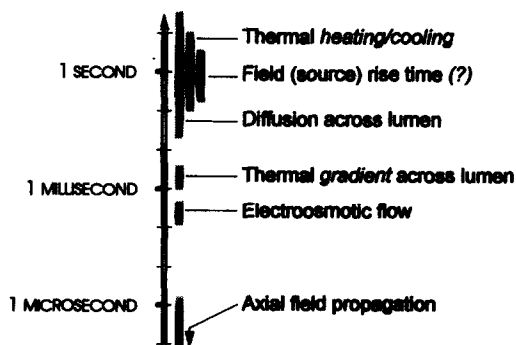

Fig. 7. Summary of timescales of CE transient processes, given here for capillary of 50 μm inside diameter, 360 μm outside diameter.

$$D_x = RTm_x/FZ_x \qquad (15)$$

where R is the ideal gas constant, T is the local temperature, F is the Faraday constant, and Z_x is the signed charge on analyte x. Note that eqn. 15 neatly accounts for the temperature dependence of the ratio D_x/m_x previously noted in experimental results [2].

We note here that the diffusion coefficient and mobility are directly linked by fundamental statistical mechanics and not through viscosity. Attributions to the contrary notwithstanding [2], we have never doubted the validity of eqn. 15. Viscosity cannot be derived from either analyte diffusion coefficients or mobilities, or *vice versa* [1], except under assumptions which are tenuous in homogeneous solution and patently invalid in the presence of gels and viscosity-enhancing polymers. One should not rely too much on any connection between ion mobility and electrolyte viscosity as is often done [2,41] but should use the Stokes–Einstein equation (15 above) instead when at all possible.

MINIMIZING THERMAL DISPERSION THROUGH POTENTIAL MODULATION

Methods

Thermal simulations demonstrate that the parabolic thermal profile in the capillary lumen rises and falls rapidly when the driving potential is applied or withdrawn, respectively, and the initial temperature changes occur rapidly and slow considerably after only a few milliseconds (Figs. 3–6). This behaviour suggests that when driving potential is applied, the ions immediately reach a nearly constant velocity, but that the dispersion-generating temperature difference between the center and the wall of the lumen requires a few milliseconds to reach its maximum. In this section we explore whether it is possible to maximize the ion migration while minimizing zone dispersion by taking advantage of the two process's different timescales. Because the disparities in the processes' time-dependent behaviour exist for only a few milliseconds, a much shorter time than any feasible CE separation requires, we are constrained to exploit it in some repetitive fashion. The applied

potential is the only whole-column experimental condition we can think of manipulating in just a few seconds. These two constraints suggest that in order to suppress the effects of thermal broadening, we investigate the use of driving potential modulation.

All repetitive modulation patterns contained only three parts, applied in this order: a period a of duration l_a during which a positive potential gradient of magnitude E_a is applied, followed by a period b of duration l_b of negative potential gradient of magnitude E_b, followed in turn by a period c of duration of l_c of zero applied potential (see Fig. 8). Rather than using the potential gradients, we found it convenient to work instead from capillary-center ballistic heating rates B_a and B_b

$$B_a = \frac{E_a^2 \Lambda_{aq} D_{aq}}{C_{p,aq}}$$

$$\qquad (16)$$

$$B_b = \frac{E_b^2 \Lambda_{aq} D_{aq}}{C_{p,aq}}$$

that one would obtain from instantaneously switching from zero potential gradient to E_a and E_b, respectively, where Λ_{aq} is the specific electrical conductivity within the electrolyte solution, D_{aq} is the electrolyte density, and $C_{p,aq}$ is the electrolyte specific heat. Our assumption that the rate k of radial thermal gradient relaxation within the electrolyte is slow compared to diffusional and column-wide heating relaxation rates is supported by results of previous sections of
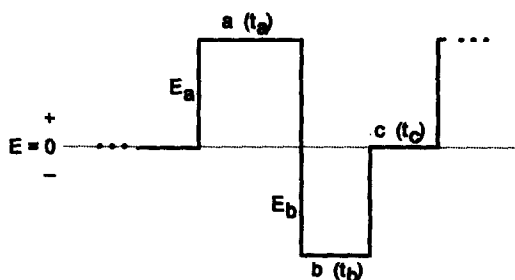

Fig. 8. Definition of potential modulation sequence used in this work. E_a and E_b are potential gradients during periods a and b, and E_a, E_b and E_c are the durations of periods a, b and c.

this work. Assuming that a single radial thermal gradient relaxation time exists implies that temperature *vs.* time curves represent exponential decays. We expect that the results of this feasibility study do not depend strongly on minor deviations from exponential relaxation curve shapes. Our assumption that the decay curves during periods *a* and *b* are exponential implies in turn that conductivity changes caused by the electrolyte temperature excursions are linear, that is, that eqn. 16 holds. This assumption is very probably valid over the few degree's temperature fluctuations expected within the lumen of real capillaries. Finally, we assume that rectangular-wave modulation patterns can in fact be delivered to the capillary, that is, that the power source can deliver high-frequency components. For a capillary of inside diameter 50 μm, k is about 500 s^{-1} (see Fig. 5). The power source must deliver alternating current components of at least a few kilohertz to synthesize a reasonable approximation of a 500-Hz square wave. Sine-wave modulation at 390 Hz [23] and reasonably square-wave modulation at 500 Hz [13] of the CE driving potential have been reported previously.

The steady state (identical thermal profiles in sequential cycles) is achieved only after very many identical modulation cycles. The present model considers only the analytes' behavior at steady state. Under the assumptions of the previous paragraph, steady-state capillary center temperatures $T_{a,t}$, $T_{b,t}$ and $T_{c,t}$ during periods *a*, *b* and *c* are given by

$$T_{a,t} = T_{a,\infty} - T_{a,\infty}\, e^{-k(t - t_{a,0})}$$

$$T_{b,t} = T_{b,\infty} + (T_{a,\infty} - T_{b,\infty})\, e^{-k(t - t_{b,0})} \qquad (17)$$

$$T_{c,t} = T_{b,\infty}\, e^{-k(t - t_{c,0})}$$

where $T_{a,\infty}$ and $T_{b,\infty}$ are the asymptotic capillary-center temperatures, relative to ambient temperature, at times long compared to the intralumen thermal relaxation time k^{-1} but short compared to the column-wide thermal relaxation time, and where $t_{a,0}$, $t_{b,0}$ and $t_{c,0}$ are times at the beginning of periods *a*, *b* and *c*, respectively, within a given cycle. One can solve by substitution for the capillary-center temperatures $T_{a,0}$,

$T_{b,0}$ and $T_{c,0}$ at potential-switching times $t_{a,0}$, $t_{b,0}$ and $t_{c,0}$ to obtain

$$T_{a,0} = T_{a,\infty} + (T_{c,\infty} - T_{a,\infty})\, e^{-kt_a}$$

$$T_{b,0} = \frac{T_{b,\infty}(1 - e^{-kt_b}) + T_{a,\infty}\, e^{-kt_b}(1 - e^{-kt_a})}{1 - e^{-kt_a}\, e^{-kt_b}\, e^{-kt_c}} \qquad (18)$$

$$T_{c,0} = T_{b,\infty}\, e^{-kt_c}$$

To judge the success of any given modulation sequence defined by B_a, B_b, kt_a, kt_b and kt_c requires that one integrate over one steady-state modulation cycle the capillary-center displacement of analyte x with velocity temperature coefficient j_x relative to its displacement at the capillary wall, assuming that electroosmotic flow is either absent, laminar, or relaxing radially much faster than radial thermal relaxation. This dispersion-generating net displacement difference Δd_x is

$$\Delta d_x$$

$$= j_x\left\{ B_a \int_0^{t_a} (T - T_{a,0})\, \mathrm{d}t + B_b \int_0^{t_b} (T - T_{b,0})\, \mathrm{d}t \right\}$$

$$= j_x\{ B_a[T_{a,\infty}t_a - (T_{c,0} - T_{a,\infty})(e^{-kt_a} - 1)/k]$$

$$- B_b[T_{b,\infty}t_b - (T_{a,0} - T_{b,\infty})(e^{-kt_b} - 1)/k]\} \qquad (19)$$

Our strategy is thus to explore modulation sequences giving zero net axial displacement difference Δd_x, selecting for further consideration those which yield significant net forward displacement. Because modulation sequences vary in duration, we found it most useful to compare the usefulness of modulation sequences with zero Δd_x by comparing values of R_d, the ratio of $d_{\max}$, the forward displacement one would achieve by applying a constant potential equal to the modulation sequence's maximum potential, to d_{mod}, the forward displacement under modulation.

$$R_d = \frac{d_{\max}}{d_{\mathrm{mod}}} = \frac{(t_a + t_b + t_c) \cdot \max(|E_a|, |E_b|)}{||t_a|E_a| - t_b|E_b||}$$

$$= \frac{(t_a + t_b + t_c) \cdot \max(B_a, B_b)}{|t_a B_a - t_b B_b|} \qquad (20)$$

This measure of comparison is conservative in that it disfavors modulation sequences relative to constant potentials because capillary-center temperatures under modulation will generally not rise as high as they would under a given sequence's maximum potential held constant.

Results and discussion

The minimum set of properly scaled and dimensionless parameters defining a modulation sequence is: B_b/B_a, kt_a and kt_b. The absolute magnitudes of B_a and B_b are unimportant if the maximum applied potentials are small enough that ion velocity temperature coefficients are constant. The dimensionless duration of the zero-potential (cooling) period, defined by kt_c, is adjusted to set Δd_i to zero, so kt_c is only a dependent parameter of the modulation cycle's definition. For many combinations of B_b/B_a, kt_a and kt_b values there exists no positive kt_c yielding zero Δd_i.

We find that under this model there do exist modulation sequences that completely suppress thermally generated CE zone dispersion (Table IV). The optimal sequence appears to have the parameters $B_b/B_a = 1.0$, $kt_a = 1.5$ and $kt_b = 1.0$. This is probably a global optimum, as the range of parameters allowing for zero calculated thermal dispersion is very limited.

These sequences work because most of the

forward displacement during period a occurs when the radial thermal gradients are small, and most of the reverse displacement during period b occurs when the radial thermal gradients are fully developed. Thus, if the applied potential in the two periods are of equal magnitude, t_a may be longer than t_b, so that while the axial dispersion in the two periods exactly cancel, there is net forward ion migration.

Whether one can achieve such zone sharpening in practice we cannot say due to the number of assumptions we were required to make. To remove the assumption that relaxation is exponential in time and to explore more realistic, non-rectangular waveforms with fewer high-frequency components would require micrometer-resolution, two-dimensional (axial and radial), time-dependent integration in ion velocity and temperature, and perhaps in electroosmotic flow. Further, there has been reported experimental evidence of *radial* ion migration under modulated applied potentials [23,42] whose inclusion would complicate matters still further. Such complete integrations would be computationally demanding in the extreme.

However, because the present model's simplifying assumptions are probably close to reality, we speculate that there may exist real modulation sequences which are accessible experimentally and which suppress the dispersive effects of radial thermal gradients. We note an interesting previous report of similar suppression results obtained by introducing a steady-state retrograde hydrodynamic flow [43].

Sequences such as the ones presented herein would be most valuable when applied to highly conductive electrolyte solutions or perhaps to capillaries with large inside diameters, provided the model's timescale assumptions still apply. Preparative CE of large molecules (with small diffusion coefficients) might best make use of the proposed method. We have had to make a considerable number of assumptions in the interest of mathematical tractability. It is not clear whether the thermal states generated by optimal sequences will be near enough to steady state that exponential decay will be a useful approximation [12]. Thus, nothing can take the place of careful experimental demonstration, including

TABLE IV

SOME MODULATION SEQUENCES GIVING ZERO CALCULATED THERMAL DISPERSION

Adjustable parameters			Results	
B_b/B_a	kt_a	kt_b	kt_c	R_d
1.00	1.1	1.0	0.22	23.2
	1.2		0.46	13.3
	1.3		0.72	10.1
	1.4		1.04	8.6
	1.5		1.48	8.0[a]
	1.6		2.18	8.0[a]
	1.7		5.9	12.3
	1.8		[b]	[b]

[a] Very near apparent global optimum.
[b] No kt_c value gives zero calculated thermal dispersion.

error analysis, of this proposed antibroadening effect.

REFERENCES

1 R.-L. Chien and D.S. Burgi, *Anal. Chem.*, 64 (1992) 489A–496A.
2 S.L. Delinger and J.M. Davis, *Anal. Chem.*, 64 (1992) 1947–1959.
3 X. Huang, W.F. Coleman and R.N. Zare, *J. Chromatogr.*, 480 (1989) 95–110.
4 K.D. Altria and C.F. Simpson, *Anal. Proc.*, 23 (1986) 453–454.
5 C.L. Rice and R. Whitehead, *J. Phys. Chem.*, 69 (1965) 4017–4024.
6 J.M. Davis, *J. Chromatogr.*, 517 (1990) 521–547.
7 H.T. Rasmussen and H.M. McNair, *J. Chromatogr.*, 516 (1990) 223–231.
8 J.H. Knox and I.H. Grant, *Chromatographia*, 24 (1987) 135–143.
9 J.H. Knox, *Chromatographia*, 26 (1988) 329–337.
10 J.C. Reijenga, G.V.A. Aben, T.P.E.M. Verheggen and F.M. Everaerts, *J. Chromatogr.*, 260 (1983) 241–254.
11 M. Martin and G. Guiochon, *Anal. Chem.*, 56 (1984) 614–620.
12 H.S. Carslaw and J.C. Jaeger, *Conduction of Heat in Solids*, Clarendon Press, Oxford, 2nd ed., 1959, Ch. 7 and appendix 4.
13 D.N. Heiger, S.M. Carson, A.S. Cohen and B.L. Karger, *Anal. Chem.*, 64 (1992) 192–199.
14 T.M. Olefirowicz and A.G. Ewing, *Anal. Chem.*, 62 (1990) 1872–1876.
15 R.A. Wallingford and A.G. Ewing, *Anal. Chem.*, 60 (1988) 1972–1975.
16 H.K. Jones, N.T. Nguyen and R.D. Smith, *J. Chromatogr.*, 504 (1990) 1–19.
17 J.F. Brown and J.O.N. Hinckley, *J. Chromatogr.*, 109 (1975) 218–224.
18 M. Jansson, Å. Emmer and J. Roeraade, *J. High Resolut. Chromatogr.*, 12 (1989) 797–801.
19 T. Tsuda, J.V. Sweedler and R.N. Zare, *Anal. Chem.*, 62 (1990) 2149–2152.
20 J.F. Brown and J.O.N. Hinckley, *J. Chromatogr.*, 109 (1975) 225–231.
21 D.J. Harrison, A. Manz, Z. Fan, H. Lüdi and H.M. Widmer, *Anal. Chem.*, 64 (1992) 1926–1932.
22 A. Manz, D.J. Harrison, E.M.J. Verpoorte, J.C. Fettinger, A. Paulus, H. Lüdi and H.M. Widmer, *J. Chromatogr.*, 593 (1992) 253–258.
23 C.-Y. Chen, T. Demana, S.-D. Huang and M.D. Morris, *Anal. Chem.*, 61 (1989) 1590–1593.
24 J.O.N. Hinckley, *J. Chromatogr.*, 109 (1975) 209–217.
25 H. Wätzig, *Chromatographia*, 33 (1992) 445–448.
26 A. Vinther and H. Søeberg, *J. Chromatogr.*, 559 (1991) 27–42.
27 R.J. Nelson, A. Paulus, A.S. Cohen, A. Guttman and B.L. Karger, *J. Chromatogr.*, 480 (1989) 111–127.
28 E. Grushka, R.M. McCormick and J.J. Kirkland, *Anal. Chem.*, 61 (1989) 241–246.
29 M. Coxon and M.J. Binder, *J. Chromatogr.*, 101 (1974) 1–16.
30 M.S. Bello and P.G. Righetti, *J. Chromatogr.*, 606 (1992) 103–111.
31 M.S. Bello and P.G. Righetti, *J. Chromatogr.*, 606 (1992) 95–102.
32 C.-W. Whang and E.S. Yeung, *Anal. Chem.*, 64 (1992) 502–506.
33 R.S. Rush, A.S. Cohen and B.L. Karger, *Anal. Chem.*, 63 (1991) 1346–1350.
34 A.E. Jones and E. Grushka, *J. Chromatogr.*, 466 (1989) 219–225.
35 Y. Kurosu, K. Hibi, T. Sasaki and M. Saito, *J. High Resolut. Chromatogr.*, 14 (1991) 200–203.
36 G.O. Roberts, P.H. Rhodes and R.S. Snyder, *J. Chromatogr.*, 480 (1989) 35–67.
37 M.J. Sepaniak and R.O. Cole, *Anal. Chem.*, 59 (1987) 472–476.
38 S. Terabe, K. Otsuka and T. Ando, *Anal. Chem.*, 57 (1985) 834–841.
39 S. Terabe, K. Otsuka and T. Ando, *Anal. Chem.*, 61 (1989) 251–260.
40 T.T. Lee and E.S. Yeung, *Anal. Chem.*, 64 (1992) 1226–1231.
41 H.J. Issaq, I.Z. Atamna, G.M. Muschik and G.M. Janini, *Chromatographia*, 32 (1991) 155–161.
42 T. Demana, U. Guhathakurta and M.D. Morris, *Anal. Chem.*, 64 (1992) 390–394.
43 W.A. Gobie and C.F. Ivory, *J. Chromatogr.*, 516 (1990) 191–210.